


RESEARCH ARTICLE

Online cracking detection by means of optical techniques in laser-cladding process

Aitor García de la Yedra¹  | Michael Pflieger² | Benat Aramendi¹ | Marcos Cabeza¹ | Fidel Zubiri¹ | Thomas Mitter² | Bernhard Reitingner² | Edgar Scherleitner²

¹Smart Manufacturing, IK4-LORTEK, Ordizia, Spain

²LUS Department, RECENDT GmbH, Linz, Austria

Correspondence

Aitor García de la Yedra, Smart Manufacturing, IK4-LORTEK, Arranomendia 4A, Ordizia 20240, Spain.
Email: agarciadelayedra@lortek.es

Funding information

H2020 European Institute of Innovation and Technology, Grant/Award Number: 636902; Strategic Economic-Research Program; European Regional Development Fund (ERDF); Federal Government of Upper Austria; Talleres Mecánicos; European Community's HORIZON 2020 Programme (H2020-FoF-2014)

Summary

Additive manufacturing processes are advanced production methods used to build parts layer by layer or to repair components. One of the common limitations of this type of processes is the presence of defects that may cause failure of the part. In order to avoid this undesirable situation, quality control is essential. This is typically performed postprocess, once the part has been manufactured. However, online quality control systems would bring great benefits to detect the defects whereas they occur. In this work, a novel method is presented based on three online monitoring systems; thermal imaging and two different acoustic emission sensors. The results given by these methods are compared with traditional inspection procedures and validated by microscopic analysis. Results reveal the effectiveness of the procedure for detecting two different cracking mechanisms and also to determine values above which no layer cracking occurs.

KEYWORDS

acoustic emission, cladding, interferometry, thermography

1 | INTRODUCTION

Laser cladding is a surface modification technique, which is being extended considerably to industry applications during the last years. It is a melting process in which a laser is used to fuse an alloy onto a substrate improving wear and corrosion resistance of the coating. However, its further development is being restricted in some cases due to the appearance of defects and more specifically due to cracking events.

Substrate preheating helps to reduce the high-thermal gradients originated during the process and, thus, making the process less susceptible to cracking. However, the quality control of the process is still essential to ensure structural integrity of the manufactured parts. In this regard, nondestructive techniques (NDTs) play an important role to verify that the material is free of cracks (and to avoid these flaws propagation during service). A common approach deals with the use of liquid penetrant or magnetic particles testing; however, these techniques have some drawbacks. Among them, they consist of manual procedures with very low chances of automation, and the inspection is carried out once the part has been manufactured without any possibility of taking corrective measures. In order to overcome these limitations, the use of acoustic emission (AE) sensors has increased in the last years, not only in cladding but also in some other manufacturing processes including 3-D additive manufacturing.¹⁻³

AE refers to the generation of transient elastic waves produced by a sudden redistribution of stress in a material. This energy release, in the form of stress waves, propagates to the surface and is recorded by passive piezoelectric sensors.

There are two different ways in which an AE may be analyzed: Wave propagation-based analysis to identify the source and location of the defect (by using two or more sensors) and the traditional technique that captures emission parameters such as emission counts, peak levels, and energies as defined in Figure 1.⁴ The former is considerably more difficult, and due to this fact, the traditional approach is more employed by researchers. In this latter approach, emission parameters can be correlated with defect formation and failures. For instance, it is well-known that during crack propagation tests,¹ the AE count rate increases as the crack growth rate increases. Similarly, the amplitude of the emission is proportional to the velocity of crack propagation and the amount of surface area created.

It may be stated that AE is a consolidated NDT method as several studies confirm. Stranza et al., for instance, focused on detection, characterization, and location of fatigue cracks in titanium samples and its propagation.⁵ Gutkin et al. investigated damage propagation in composite materials by pattern recognition of AE signals and their corresponding frequency content.⁶ With respect to Laser-Based Manufacturing processes, Gaja et al. monitored laser metal deposition process layer by layer with the purpose of detecting pores and cracks. They propose a novel system that is able to detect and classify defects in real time based on their acoustic fingerprint.² Similarly, there are some good examples of faults detection for welding,⁷ cutting, and drilling⁸ processes.

Therefore, the use of AE sensors in manufacturing is well established, in fact in some cases, it was shown to be a useful tool for laser metal deposition process. In spite of that, the conventional transducers are contacting devices with a limited bandwidth. Due to this, water cooling may be required because of the contact between the hot sample and the sensor. In some other cases, access to the part may be difficult, and thus, noncontact sensors would bring great benefits with respect to the defined approach. In this paper, two contactless photoacoustical methods are presented. One of them relies on measuring the surface displacement during the cladding process by laser interferometry, whereas the other method is based on optical detection of air-coupled ultrasound emitted from the part. These sensors offer a higher signal bandwidth than the conventional AE sensors, and they are less problematic and more flexible because they are operated contactless. The use of vibrometric sensors may be dated back to 90's,⁹ but the application in additive manufacturing processes may be considered novel. The second method has been developed recently¹⁰ and constitutes a completely new approach to acoustic process monitoring.

In order to prove this development, several cladding tests were defined under different conditions (prewarming temperature, process parameters, substrate material...) to foment different types of cracking. Additionally, online thermal monitoring was performed to relate thermal gradients to acoustic signals and, hence, to susceptibility to cracking. For validation purposes, microscopic investigations were conducted after cladding process as well as liquid penetrant testing to match acoustic signal results with conventional NDTs. This analysis supported the study of the cracking behaviour as well as the system reliability.

2 | EXPERIMENTAL PROCEDURE

2.1 | Cladding process experiments

For the development of this work, valve seats from the gas and oil industry were manufactured. These samples were of circular shape (220-mm diameter and 50-mm thick) with an inner groove, which is the area to be filled up by applying

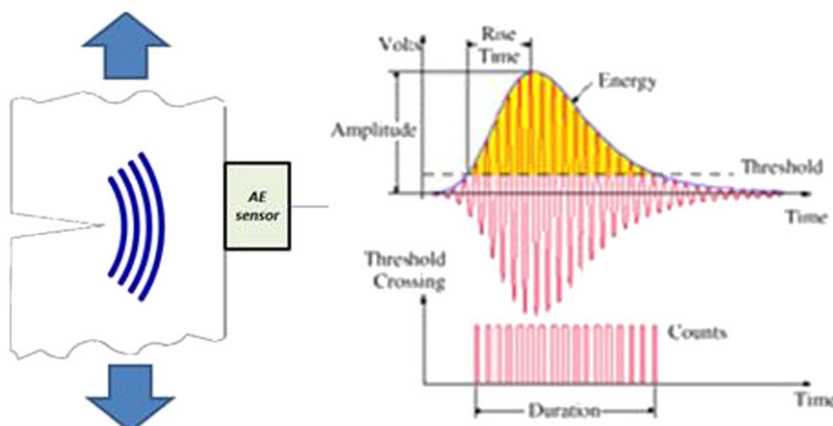


FIGURE 1 Scheme of a simple acoustic emission setup (image on the left) and definition of acoustic emission events (image on the right) based on typical cracking phenomena

two Stellite 6 layers (see chemical composition in Table 1). Two different substrates or base materials were employed: low-carbon steel and medium-carbon steel, being the hardness of this latter considerable higher. This made it more prone to cracking in the heat-affected zone (HAZ) area. In addition to this HAZ cracking, manufacturing conditions cause severe thermal stresses, and in case no further measures are taken—as substrate preheating—the layer cracks. Even if the substrate is preheated, the absence of cracking needs to be ensured by an NDT technique as in this work, where acoustic emission based systems were employed (Figure 1). Therefore, these tests foment two types of cracking: HAZ cracking due to material hardness and layer cracking due to thermal stresses. Figure 2 shows the facility in which tests were carried out, the raw part and the final part after cladding process.

The aim of this work is to determine the quality of the cladding process online, by applying different contactless testing methods. Therefore, two measurement series were performed; the former was aimed at the validation of noncontact AE sensors for detecting different cracking mechanisms. The second series were performed for the cross-correlation with another sensor and optical microphone.

In the first series, substrates at room temperature and in a preheated state (heated up in an industrial oven to 250°C) were manufactured for comparison purposes. In addition, cladding process parameters such as laser power, powder feed rate, and travel speed were modified resulting in different heat input into the process (Table 2). All tests were monitored by a laser vibrometer (Bossa Nova), detecting the AE in form of vibrations directly on the sample surface. In addition, a thermal camera (microbolometer, Flir model) measured the temperature distribution within the melt pool and its surroundings (Figure 3a).

For the second test series, five substrates at room temperature were used (see Table 3). In this case, the laser vibrometer (Bossa Nova) was employed in combination with the optical microphone (Xarion), both in order to detect AE. This latter is more compact, smaller, and more suitable for industrial applications such as the cladding process.¹¹ Thus, the aim of these test series was to compare its performance in terms of detection capability.

After each test, the samples are placed into a sepiollite container to guarantee a homogeneous cooling process—reducing the risk of cracking after the process. This was performed so that the acoustic signals could be correlated with

TABLE 1 Chemical composition of the employed materials

Material	Stellite 6 (%)
Fe	<1
C	1.2
Cr	30
W	5
Co	Base

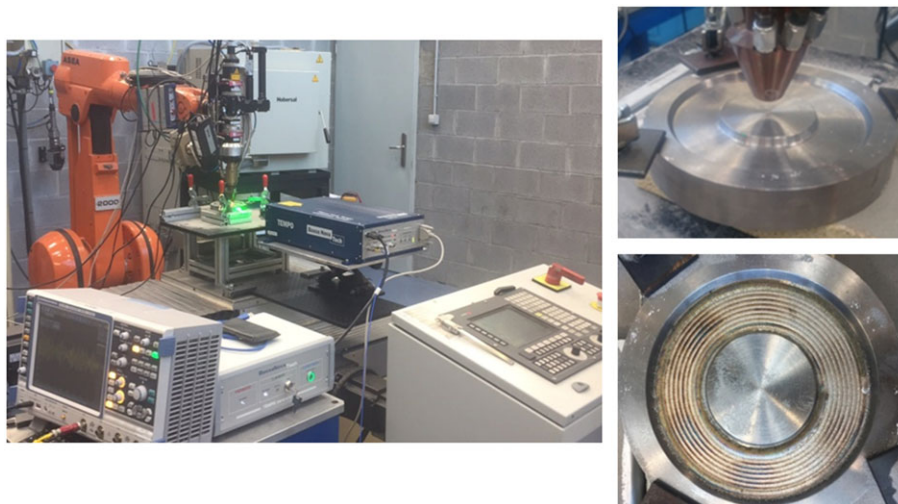
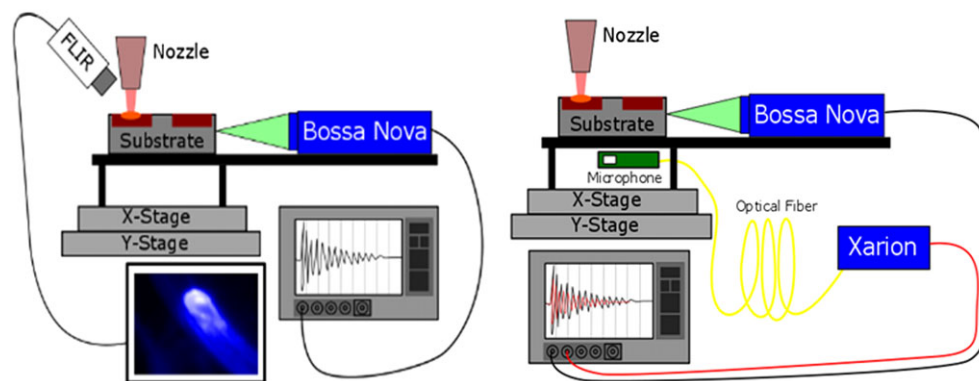


FIGURE 2 Experimental setup for the cladding process; (a) general view of the facilities, (b) sample and nozzle employed for cladding, and (c) final part

TABLE 2 List of tests for the validation of crack-monitoring system

Test	Preheating (°C)	Substrate material	Laser power (W)	Travel speed (mm/min)	Powder feed rate (g/min)
1	None	Low carbon	3,000	1,700	40
2	None	Low carbon	2,700	1,700	40
3	None	Low carbon	2,700	1,200	40
4	None	Low carbon	2,700	1,200	26
5	None	Low carbon	2,700	1,700	26
6	250	Medium carbon	2,700	1,700	40
7	250	Medium carbon	2,700	1,200	40
8	250	Medium carbon	2,700	1,200	26
9	250	Medium carbon	2,700	1,700	26

**FIGURE 3** Measurement scheme of the two test series; a) first test series and b) second test series**TABLE 3** List of tests for optical microphone-laser vibrometer comparison

Test	Preheating (°C)	Substrate material	Laser power (W)	Travel speed (mm/min)	Powder feed rate (g/min)
1*	None	Low carbon	2,700	1,700	40
2*	None	Low carbon	2,700	1,700	40
3*	None	Low carbon	2,700	1,700	40
4*	None	Low carbon	2,700	1,700	40
5*	None	Medium carbon	2,700	1,700	40

liquid penetrant tests because the detected cracks by AE were recorded during the process and not during cooling. However, it has to be stated that the maximum likelihood for defects appearance is given during the process or just after the process is finished—during the initial phase of the cooling when thermal gradients are higher. That is, what is ensured with this procedure is that all cracking events occur whereas the sensor is active.

The manufacturing process consists of filling up the circular groove with two layers by a spiral rotation (see Figure 2). The thermal camera was attached to the cladding head in order to monitor the melt pool area and its surroundings. On the other side, the laser vibrometer and the optical microphone were attached to the moving part of the system; this way, any acoustic signal induced by the process was detected at the same spot of the substrate surface.

In the first test series, the parts were manufactured by applying different process parameters to show the influence on the quality of the part. On the other side, in the second test series, the process parameters were kept constant to show the applicability of the optical microphone and compare this method to the laser vibrometer. The process parameters are listed in Table 3.

2.2 | Photoacoustic and thermal signals acquisition

During laser deposition process, the AE was measured by two different contactless methods. The main method in this work was a laser vibrometer based on a two-wave mixing interferometer¹²; the Tempo by Bossa Nova, which has been proved to be very efficient in difficult applications such as NDT inspection via laser ultrasound. With this system, the displacement of the surface of the clad part is measured. This is performed by aiming the measurement head at the lateral side of the sample. Thereby, the AE caused by the cladding process is measured continuously.

The second method used in this work to measure the AE is a membrane-free optical microphone, the Eta250 Ultra by Xarion. This contactless principle consists of a membrane-free microphone based on a Fabry–Perot laser interferometer. This method allows acquiring acoustic signals up to 1 MHz bandwidth and changes of the refractive index below 10^{-14} , corresponding to pressure changes of 1 μPa .

In the second test series, both methods were used simultaneously, this time triggered by the optical microphone. This second method was used to verify the data gathered from the first series and to show the feasibility of the optical microphone as a tool for monitoring the process.

For data acquisition, the background noise was determined by measuring the AE during movement of the sample without starting the deposition process. This means that the CNC program was executed whereas the powder and laser were disabled. From these measurements, the trigger level was set slightly above this value (around 12 mV). Another parameter defined in foregoing test measurements is the length of a recorded acoustic signal. It was observed that strong acoustic events can take up to 8 ms, and therefore, the record length was established a bit longer; 10 ms. With respect to the thermal signal acquisition, as previously mentioned, a microbolometer-based camera was used, which is sensitive in the long wave infrared region; 7–12 μm . From thermal images, several features may be extracted (melt pool shape, thermal radiation values, etc.). In this research, substrate temperature was measured online by image processing as illustrated in the sequence of Figure 4. This decision was made so as to be capable of correlating cracking events with temperature values. Layer cracking is directly linked to thermal stresses, and this is why substrate temperature is relevant (layer-cracking likelihood is higher with lower substrate temperature). This is measured in arbitrary units because for real temperature values, emissivity values are required, which depend on temperature, oxidation state, surface roughness, and some other factors that are not well-understood.^{13,14}

It is interesting to note the complementary approach presented in this work; on the one side, AE sensors provide information about an instantaneous state of the sample (such as cracking event) at any location of the part. On the other side, thermal imaging reveals continuous information related to the surface of the part, which is one of the main causes of layer-cracking mechanisms. Therefore, this work aims to take advantage of this complementary aspect to better understand and detect the cracking phenomena.

2.3 | Microscopic analysis and liquid penetrant testing

After samples manufacturing, liquid penetrant testing was conducted in order to determine the results in terms of a number of defects. In addition, after that, the cladding layer was machined up to 0.5-mm depth as it is done in the real

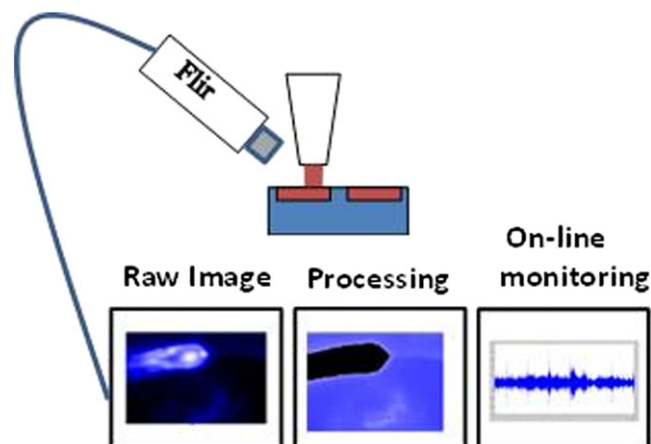


FIGURE 4 Measurement scheme of thermal signals

application of these parts. This is when conventional nondestructive methods are applied through liquid penetrant testing, after machining. The same procedure was followed for the sake of comparison with the approach suggested in this study. Moreover, some of the samples were cut, and cross-sections were prepared to perform microscopic studies and cracking behaviour analysis.

3 | RESULTS AND DISCUSSION

The signals detected by the laser vibrometer and by the optical microphone were examined in the same way. As previously stated, each acoustic signal caused by the cladding process resulting in signal amplitude higher than the corresponding threshold is recorded for 10 ms in length. The sum of the squared amplitudes within this 10 ms is a measure of the energy of this particular event, as illustrated in the following formula.

$$\text{Acoustic Energy} = \int_0^{10} (I(t))^2 dt \quad (1)$$

This value and the maximum amplitude of the event are the most relevant figures for further analysis. The following graph shows the number of events and their acoustic energy measured during one cladding process (see Figure 5).

In the mentioned graph, the x-axis represents the number of events, whereas the y-axis corresponds to the acoustic energy values. In this data set, the number of events is high (around 500), which does not mean that there were as many cracking phenomena as event numbers. The events are a combination of peaks (figure on the left) and the so-called background noise (figure on the right). The high peaks refer to initial cracking or crack growth. The background noise is a sign of the internal stress. In this case, the noise presents a trend towards higher values whereas the second layer is deposited. This gives a clear sign of an internal stress increase during the deposition of the second layer.

3.1 | Comparison between non-preheated and preheated parts

With the above-described signals, a comparison between preheated and non-preheated samples was performed. The non-preheated ones tend to crack in the cladding layer due to thermal stresses. The outcomes of these tests are compared in order to analyze the capability of the different methods to predict cracking events.

With regard to thermal imaging, the substrate temperature during the process shows—as expected—a clear relation with the probability of cracking. According to the results of liquid-penetrant testing, no layer cracks were revealed within the cladding of substrates 6–9. For the rest of the cases—from 1 to 5—at least one crack was detected by the inspection. By the correlation of the number of cracks with the mean substrate temperature during the process, a minimum temperature is obtained, above which no layer delamination occurs (Figure 6; dashed line). This highlights the influence of the thermal gradients on the quality of the process and the importance of monitoring the substrate temperature.

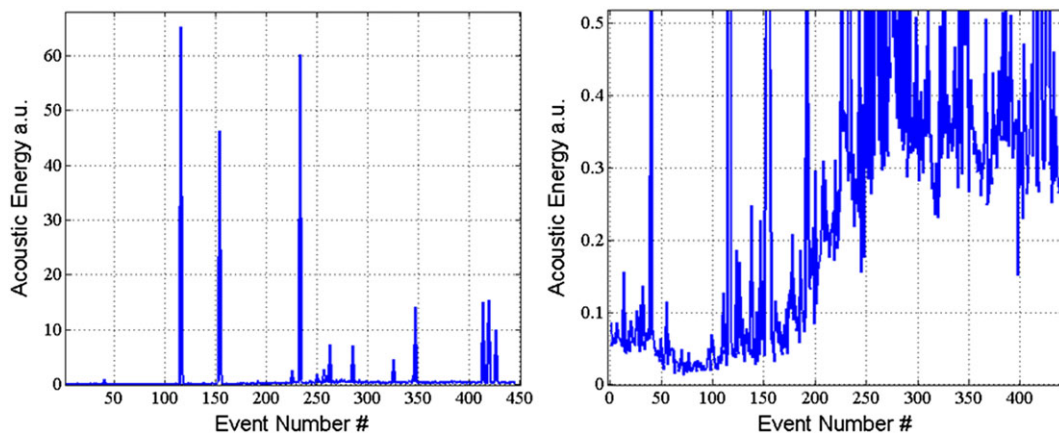


FIGURE 5 Acoustic emission signals example revealing clear crack evidence (as high-amplitude signals, figure on the left) and background noise level (figure on the right)

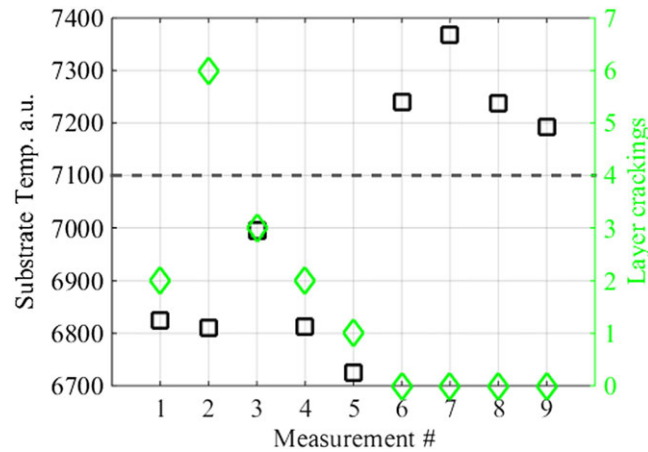


FIGURE 6 Correlation of the mean substrate temperature (black squares) versus the number of layer cracking found by liquid-penetrant testing (green diamonds) for each measurement

The comparison of the acoustic signals leads to similar conclusions. Figure 7 illustrates two data sets as an example; one preheated-crack-free sample (red) and one non-preheated-cracked sample (blue). In the data set of the preheated substrate, the number of events is considerably reduced, from 120 to 55. But the more important feature is the energy value of the spikes, which is one order of magnitude higher in the cracked sample, whereas in the “sane” crack free

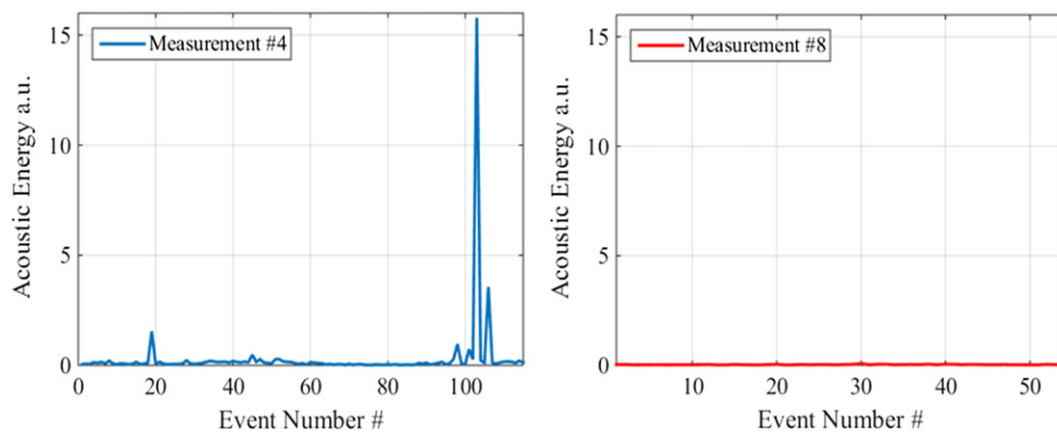


FIGURE 7 Comparison of two acoustic emission data sets without preheating (left row, measurement 4) and with preheating (right row, measurement 8)

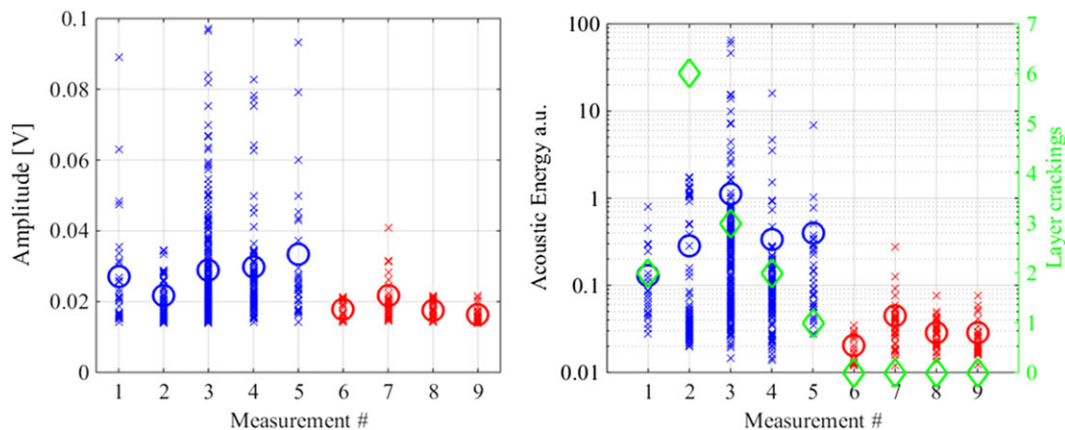


FIGURE 8 Comparison of amplitude (graph on the left) and acoustic energy (graph on the right) correlated with the number of layer delaminations detected by liquid-penetrant testing method (green diamonds) for each of the nine measurements; cold (blue) and preheated (red) substrates. Cross symbolizes a single event and the circle the averaged value for the whole cladding process

sample, the amplitude levels are around process background noise. Therefore, these peaks clearly represent cracking events. When comparing the number of these peaks with the number of cracks revealed by the conventional inspection, it is found that the liquid penetrant test underestimates the number of cracks. This may be due to two reasons; on the one hand, the inspection is performed after the cladding process, and shallow cracks that appear in the first layer may be covered in the second one. On the other hand, the conventional inspection may not be able to reveal the smallest cracks.

For a better comparison of the nine AE data sets of this serie, the amplitude (Figure 8, left) and the corresponding acoustic energy (Figure 8, right) of each event upon the trigger level for each measurement are shown. In these graphs, the maximum amplitude of each particular event is plotted as a cross and the averaged value of the whole data set as a

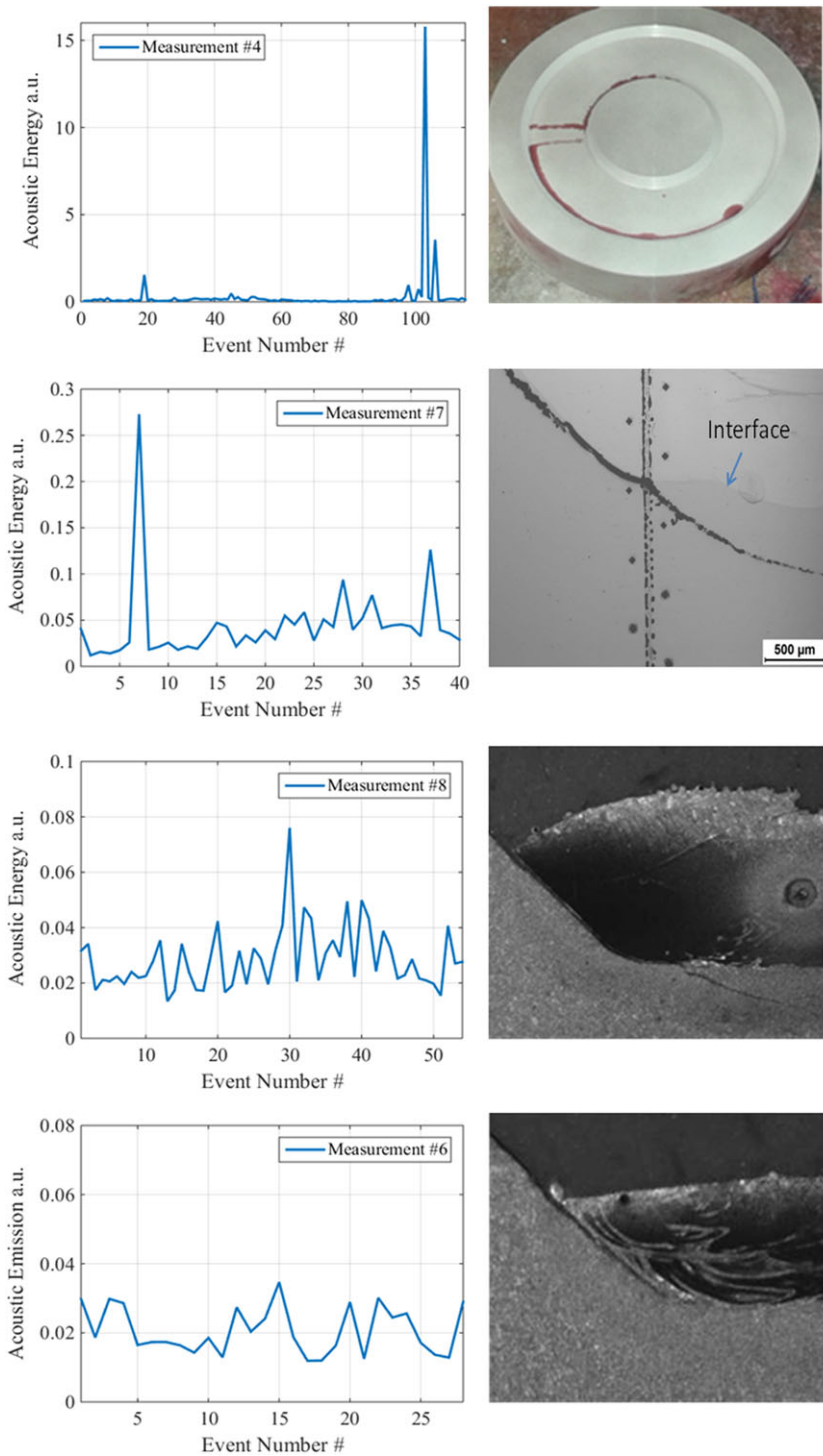


FIGURE 9 Correlation between acoustic emission data sets (left column) and liquid penetrant respectively microscopic analysis (right column) for different cases: (a) Layer cracking (low-carbon substrate; cold), (b) heat-affected zone cracking—surface breaking—(medium-carbon substrate; preheated), (c) small-heat-affected zone cracking, and (d) crack free sample

circle. In a similar to thermal signals (Figure 6), the data given by the laser vibrometer also shows a good correlation with the cracks proven by liquid penetrant testing (Figure 8, right, green diamonds). By having a look at the mean values for maximum amplitude and acoustic energy, it is evident that the measurements performed on the cold substrates (blue 1–5) show higher values.

With respect to maximum amplitude and the acoustic energy for the single events (indicated as crosses in the graph), these values vary in a wider range compared with the preheated samples. This is due to the higher temperature gradients present in the cold samples, which cause higher tensions during the cladding process. This leads to a higher cracking probability and a more intense cracking process followed by a higher acoustic signal. Besides, following an initial crack, further delamination of the same crack may follow, which also leads to more AE due to a bigger fractured area.

3.2 | Detection of inner cracks: HAZ cracking

In addition to above-mentioned defects—caused due to thermal stress—two different substrate materials were employed: Low-carbon and medium-carbon alloys; the latter one is known to exhibit higher probability for cracking at the interface between the cladding layer and the substrate. It is not possible to detect this type of defect with thermal imaging. However, the acoustic signals reveal the presence of these events even though they occurred in the underlying layer. As an example, different AE data sets and their corresponding results of the conventional testing method of different defects are shown in Figure 9. First, the data set of a non-preheated low-carbon alloy substrate (measurement #4, Figure 9) is compared with the data set of a preheated medium-carbon alloy measurement #7, Figure 9).

As already mentioned, the non-preheated sample led to high-acoustic energy peak values (up to 14) ascribed to layer-cracking events as this is verified with liquid-penetrant testing (measurement #4, Figure 9). The preheated one, on the other hand, did not suffer layer cracking but HAZ cracking due to the substrate material hardness. In this case, there is one single peak but with lower acoustic energy (measurement #7, Figure 9). If the analysis is extended to the rest of the cases it is revealed that all samples exhibiting only HAZ show peaks with very low acoustic energies (0.07) except for the one that grew up to the surface. In this case, the value of the peak was considerably higher (>0.3 as mentioned previously). Looking at the dataset of the crack-free sample, the resulting acoustic energy is within the same level as the background noise (0.03 as observed in Figure 9 measurement #6). The conclusions drawn from the AE datasets are verified by liquid penetrant testing and microscopic analysis.

3.3 | Optical microphone vs. laser-Vibrometer

In this section, an alternative method (Xarion) to the optical system (Bossa Nova) is shown. Analysis of the data is done in the same way as described in Section 3.2 and 3.3. In the following plots, the data obtained by the two different contactless AE methods are compared.

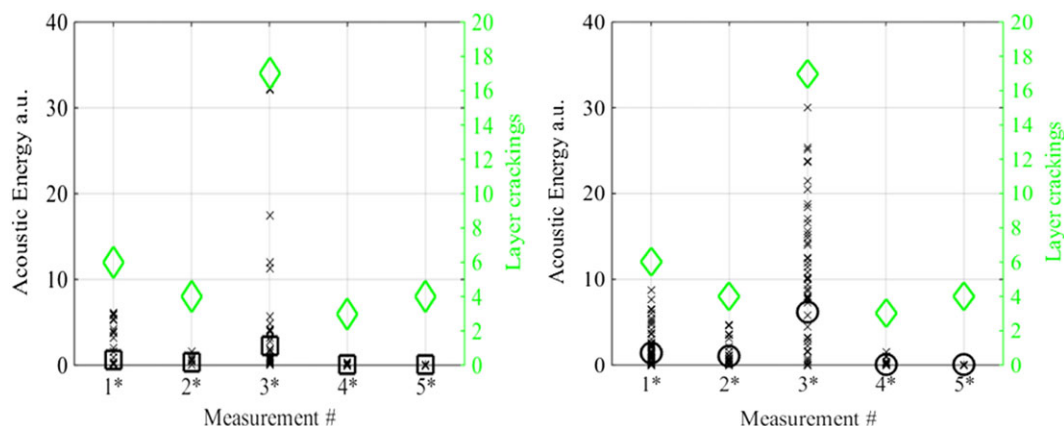


FIGURE 10 Acoustic energy for each event (cross) and mean acoustic energy (square, circle) for each measurement by the Xarion (left, square) and the Bossa Nova (right, circle) correlated with the number of layer delaminations detected by liquid penetrant testing method (green diamonds)

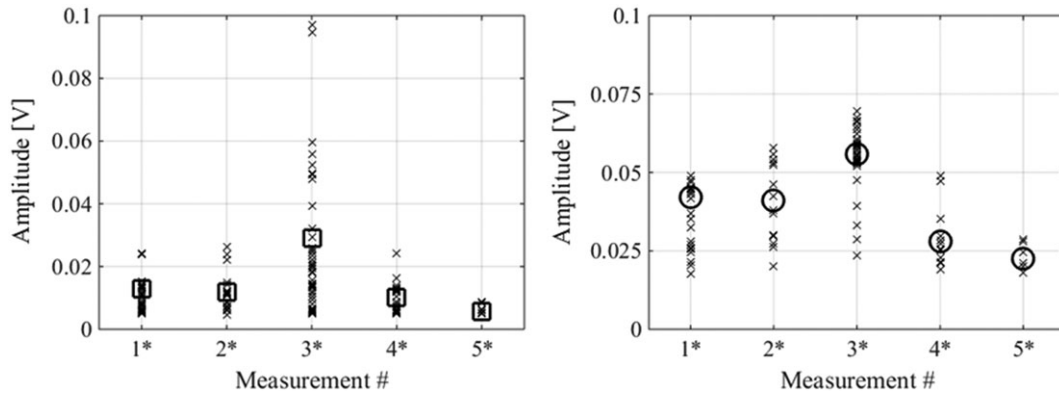


FIGURE 11 Maximum amplitude for each event (cross) and mean amplitude (square, circle) of each measurement measured by the Xarion (left, square) and the Bossa Nova (right, circle)

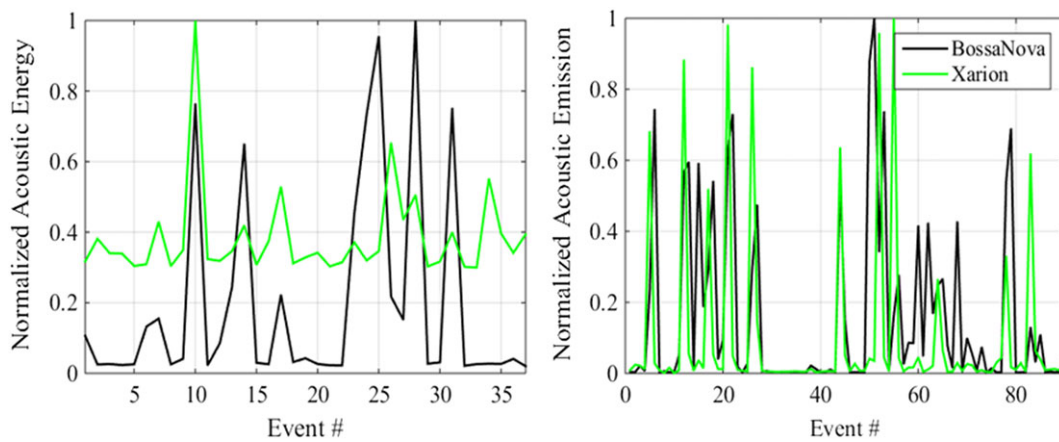


FIGURE 12 Normalized acoustic energy for each event of sample 2 (left) and sample 3 (right)

By looking at the averaged values for acoustic energy and amplitude of each measurement, it can be observed that both methods show the same tendency (Figure 10 and Figure 11). These values are also in a good correlation with the layer cracks revealed by liquid penetrant testing (green diamonds Figure 10). It has to be mentioned that, within the second test series, the number of cracks was higher than in the first test series as a result of process variability. This is one of the reasons why NDTs are required in this process to ensure that no cracking occurs.

By having a closer look at the acoustic energy of two specific measurements it is observed that both principles are sensitive to the same events. In Figure 12, the acoustic energy for each event of measurement #2* (left) and measurement #3* (right) is shown for both methods respectively. The optical microphone represented green line and the laser-vibrometer in black. For a better comparison, both datasets are normalized by their respective maximum value. It is clearly visible that in both cases individual peaks match. These results show the potential of this technique for cracking detection in laser metal deposition process.

4 | CONCLUSIONS

In this work, three different measurement methods were employed for the characterization of a laser deposition process. Data of an optical microphone, a laser-vibrometer, and a thermal camera were collected during the cladding process. In order to cause different types of cracking, process parameters and conditions were altered. Two different cracking mechanisms, layer delamination and HAZ cracking were activated through these tests. The detection of both mechanisms was demonstrated with the laser vibrometer. The optical microphone showed sufficient sensitivity to detect layer crackings, and the investigation of HAZ cracks using this device will be the subject of future work. With thermal imaging, a threshold value was found above which the parts could be manufactured free of cracks. Similarly, the AE signals clearly revealed peak values due to material fracture and energy release. The amplitude of these peaks was high due to initial

cracking and further crack growth that delaminates part of the layer and, thus, releases as much energy as the fracture area. With respect to the number of detected events, this was higher compared with conventional NDTs as liquid-penetrant testing may miss the shallowest cracks or some might be covered during second-layer deposition.

Apart from layer cracking due to thermal stresses, HAZ cracking was also detected with the laser vibrometer. In this type of cracking, crack starts at the substrate, that is, it is underlying. Therefore, unlike in layer cracking, the amplitude values were lower except for those cracks that propagate up to the surface and delaminate part of the layer creating a mix mode between HAZ and layer cracking. In this latter case, the signal was considerably higher and, therefore, more likely to be detected.

For validation purposes, these findings were compared with microscopic analysis. A good correlation was found between them as those samples free of cracks did not reveal peak amplitudes higher than the background noise. On the other hand, the samples, which had HAZ cracks showed one single peak, which is in good agreement with the single crack observed by microscopy. Thus, this work shows the great potential of optical AE and thermal imaging as an online defect detection tool.

In addition, the use of a compact optical microphone was also validated as a monitoring system for cracking detection in the cladding process. This was performed by comparing the signals from the ones obtained via the laser vibrometer. Therefore, the system may replace the conventional liquid-penetrant testing in laser-based additive manufacturing processes.

ACKNOWLEDGEMENTS

The research leading to these results has received funding from the H2020 European Institute of Technology and Innovation Programme (H2020-FoF-2014) under grant agreement 636902: COMBILASER project; *COMBination of non-contact, high-speed monitoring and non-destructive techniques applicable to LASER Based Manufacturing through a self-learning system*. Authors are also grateful to Talleres Mecánicos COMAS for the collaboration. This work has been supported by the project “multimodal and in-situ characterization of inhomogeneous materials” (MiCi) by the Federal Government of Upper Austria and the European Regional Development Fund (EFRE) in the framework of the EU-program IWB2020. This work was also supported by the strategic economic-research program “Innovative Upper Austria 2020” of the province of Upper Austria.

ORCID

Aitor García de la Yedra  <https://orcid.org/0000-0001-7776-0049>

REFERENCES

1. Wang F, Mao H, Zhang D, Zhao X, Shen Y. Online study of cracks during laser cladding process based on acoustic emission technique and finite element analysis. *Appl Surf Sci*. 2008;255(5):3267-3275.
2. Gaja H, Liou H. Defects monitoring of laser metal deposition using acoustic emission sensor. *Int J Adv Manuf Technol*. 2017;90(1-4):561-574.
3. Wu H, Yu Z, Wang YA. New Approach for Online Monitoring of Additive Manufacturing Based on Acoustic Emission. *Proc ASME 11th Int Conf Manuf Sci Eng*, Volume 3: Joint MSEC-NAMRC Symposia Blacksburg, Virginia, USA; June 27–July 1, 2016.
4. Huang M, Jiang L, Liaw PK, Brooks CR, Seeley R, Klarstrom DL. Using acoustic emission in fatigue and fracture materials research. *JOM*. 1998;50(11).
5. Strantzla M, De Baere D, Guillaume P, Van Hemelrijck D, Aggelis D. Acoustic emission monitoring of crack propagation in titanium samples. 10th International Workshop on Structural Health Monitoring, At Stanford University, Volume 1; 2015.
6. Gutkin R, Green CJ, Vangrattanachai S, Pinho ST, Robinson P, Curtis PT. On acoustic emission for failure investigation in CFRP: pattern recognition and peak frequency analyses. *Mech Syst Signal Process*. 2011;25(4):1393-1407.
7. Lee S, Ahn S, Park C. Analysis of acoustic emission signals during laser spot welding of SS304 stainless steel. *J Mater Eng Perform*. 2014;23(3):700-707.
8. Gaja H, Liou F. Automatic detection of depth of cut during end milling operation using acoustic emission sensor. *Int J Adv Manuf Technol*. 2016;86(9-12):2913-2925.
9. McBride R, Carolan TA, Barton JS, Wilcox SJ, Borthwick WKD, Jones JDC. Detection of acoustic emission in cutting processes by fibre optic interferometry. *Meas Sci Technol*. 1993;4(10):1122-1128.

10. Fischer B. Optical microphone hears ultrasound. *Nat Photonics*. 2016;10(6):356-358.
11. Fischer B, Rohringer W, Panzer N, Hecker S. Acoustic process control for laser material processing. *Laser Tech J*. 2017;12(5):22-25.
12. Drolet D, Blouin A, Neron C, Monchalain JP. Specifications of an ultrasonic receiver based on two-wave mixing in photorefractive gallium arsenide implemented in a laser-ultrasonic system. *Rev Prog Quant Nondestruct Eval*. 1996;15:637-644.
13. VAMAS. Recent Intercomparisons on Low Cycle Fatigue and Alignment Measurements. Kingston, UK: VAMAS; 2001. Report No. 41.
14. de la Yedra AG, Pedrejón JL, Martín-Meizoso A, Rodríguez R. Thermomechanical fatigue tests development and life prediction of a Nickel Base Superalloy. *Exp Tech*. 2016;40(2):777-787.

How to cite this article: García de la Yedra A, Pflieger M, Aramendi B, et al. Online cracking detection by means of optical techniques in laser-cladding process. *Struct Control Health Monit*. 2018;e2291. <https://doi.org/10.1002/stc.2291>